

1 Determining multi-scale controls on river
2 temperature: a time series approach

3 Michael Vlah

4 March 27, 2017

5 **Summary:**

6 5 data sources; watershed delineation; 2 DFAs: m=1:15, 7 covariate combina-
7 tions, 4 err. struc., 2 seasonality models; TMB; parallel computing; Bayesian
8 change/time

9 Abstract

10 Temperature is among the most important determinants of riverine biodiversity
11 and health. It is therefore a primary freshwater management concern, particu-
12 larly where cold-water fish are of high ecological, recreational, and commercial
13 value. However, river temperature in the Puget Sound watershed of the North-
14 western U.S.A. is affected by a great diversity of drivers at multiple spatial and
15 temporal scales, and little is known of their interactions. We used dynamic
16 factor analysis, a multivariate time-series technique, to examine relationships
17 among these drivers, synthesizing long-term climate and fine-scale landcover
18 data. We found that primarily rain-fed rivers experience large seasonal temper-
19 ature fluctuations, which closely track atmospheric temperature, while snow-fed
20 rivers tend to be weakly, and in some cases inversely, coupled with such fluctua-
21 tions. Among watersheds, groundwater influx, land slope, and discharge further
22 augment or dampen these relationships. Our results suggest the temperature
23 of high-elevation rivers, absent the influence of ice, should be highly variable,
24 and that glacially fed streams stand to see the largest changes in temperature
25 regime under proposed climate scenarios.

26 Introduction

27 The ecological condition of a stream or river, the life it supports, and the goods
28 and services it provides, are influenced by the timing and magnitude of seasonal
29 changes in water temperature. Temperature is a chief consideration in the man-
30 agement of fisheries, as it affects species distribution (Boisneau et al., 2008),
31 growth and reproduction (McCullough, 1999), and migration timing (Boscarino
32 et al., 2007). In particular, In the Puget Sound watershed of the American
33 Pacific Northwest, several salmonid species spawn, migrate, and emerge only
34 within the bounds of a few degrees Celsius, and thrive under even greater tem-
35 perature constraints (Carter, 2005). As a result, the success of commercial and
36 recreational fisheries that depend on the region’s riverine habitat rests on many
37 precarious factors.

38 River networks, being fractal in structure, are naturally governed by envi-
39 ronmental processes at multiple scales. Seasonal variation in water temperature
40 in rivers of the Pacific Northwest is a function of the surrounding air, as well as
41 precipitation and snowmelt (Eldridge, 1967). These drivers may in turn be me-
42 diated or supplemented by several aspects of watershed morphology at smaller
43 scales, including slope, elevation, and geology (Poole and Berman, 2001; Lisi
44 et al., 2013). Taken together, this hierarchical system complicates fishery man-
45 agement, as the temperature regime of one river may be the direct product of
46 climate, while that of another may depend more on within-watershed conditions.

47 Adding to this picture, flow regimes across rivers of the Puget Sound wa-
48 tershed vary with latitude and elevation (Reidy Liermann et al., 2012; Mauger
49 et al., 2015), and can be classified broadly into three categories by flow source
50 and hydrograph shape. Rain-dominated (RD) rivers receive little or no input
51 from snowmelt, and thus peak in discharge during the rainy season, usually be-
52 tween October and February. Snow-dominated (SD) rivers instead see peak flow
53 during spring snowmelt, often in April, May, or June. Between these extremes
54 lies a third class of rain-and-snow-driven (RS) rivers, which have appreciable
55 peaks at both times.

56 Effective management plans must therefore integrate a diversity of factors
57 across space and time in order to determine which rivers and watersheds are
58 likely to see consequential changes under projected climate and land use sce-
59 narios for the Pacific Northwest (Mote and Salathe, 2010; Radeloff et al., 2012).
60 However, the understanding required to do so is limited by knowledge of rela-
61 tionships among temperature drivers at scale.

62 We sought to identify streams in the Puget Sound region whose temperatures
63 fluctuate closely with regional trends in air temperature, precipitation, and
64 snowmelt, and those that depart from regional patterns. Our second aim was
65 to identify watershed features that correlate with such departures, and thus
66 provide a nuanced basis for predicting impacts of water temperature on aquatic
67 biodiversity and fishery health. We hypothesized that water temperature would
68 track air temperature most closely in RD rivers (Ward, 1985; Garner et al.,
69 2014). We expected deviations from this relationship to correlate best with
70 cold-water influx from snow and ice melt (Lisi et al., 2015) and with factors

71 affecting heat capacity of water, including discharge (volume over time) and
72 watershed slope (which relates to turbulence, surface area, and mixing; van
73 Vliet et al. 2013).

74 **Methods**

75 **Water and climate data**

76 We investigated climate and landscape controls on water temperature and dis-
77 charge, as separate response variables, from 1978 to 2015. Monthly time series
78 of water temperature were obtained for 24 river sites via the Washington De-
79 partment of Ecology’s River and Stream Water Quality Monitoring program
80 (Von Prause, 2017). These sites represent 19 nonnested watersheds across 9
81 counties, and range from 4 to 775 m in elevation. For at least one site at each
82 river, monthly discharge time series were also available, either from the same
83 location as one of the temperature monitoring sites, or from within 30 km on
84 the same major reach. Discharge data were aggregated by monthly mean from
85 the USGS National Water Information System database (USGS, 2017).

86

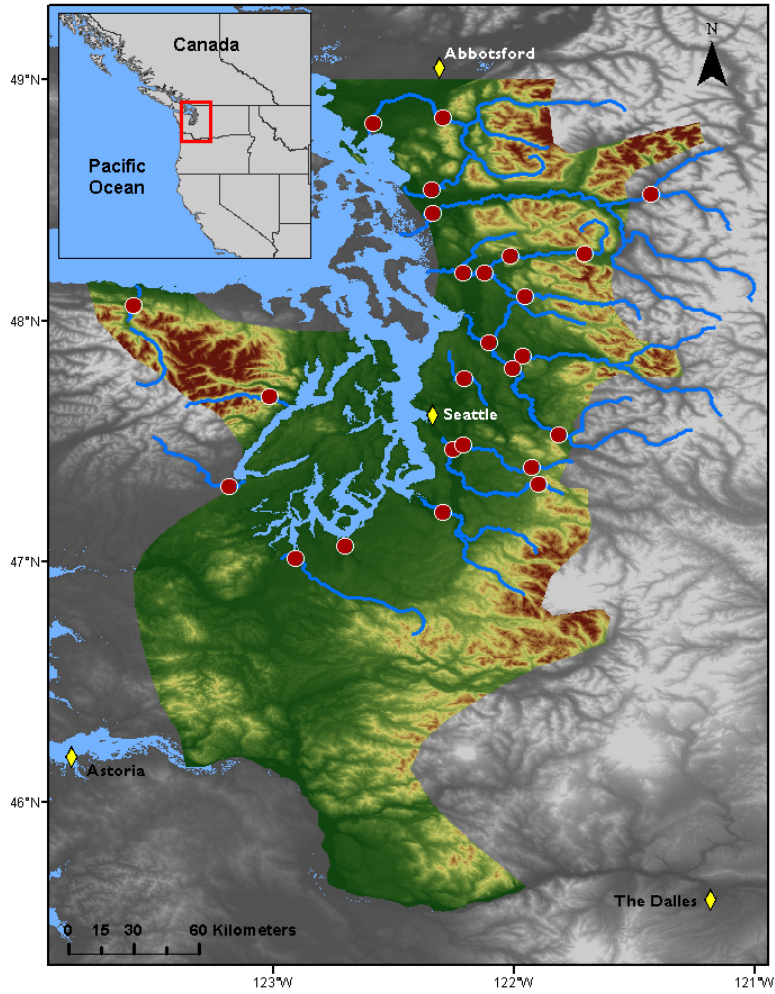


Figure 1 Site locations (red points) in relation to combined Washington State Climate Divisions 3 and 4 (colored topography), the region across which climate data were aggregated.

Potential climatic predictors of water temperature and discharge included mean and max air temperature ($^{\circ}\text{C}$), total precipitation (cm), snowmelt (cm), and hydrological drought (Palmer Hydrological Drought Index), averaged by month across the response variable time series. All but snowmelt were available through the U.S. Climate Divisional Dataset, developed by the National Cen-

ters for Environmental Information (NCEI; NOAA 2017). We acquired climatic predictor data grouped by Washington State climate division, and all but two of our sites fell within divisions 3 (Puget Sound Lowland) and 4 (East Olympic/-Cascade Foothills; see Fig. 1). We therefore aggregated these data by monthly mean across the two regions (after verifying their post-standardization similarity), resulting in a single dataset of four climatic predictor variables. A snowmelt time series was then added to this dataset, using monthly mean records from six SNOTEL sites (Bumping Ridge, Elbow Lake, Mount Crag, Park Creek Ridge, Stevens Pass, White Pass) listed by the USDA’s Natural Resources Conservation Service; USDA 2017. We calculated monthly snowmelt for each site as the absolute value of negative differences in cumulative snow water equivalent from each month to the next. The snowmelt time series was assigned zeros for any positive differences (accumulations).

Time series analysis

Response time series were modeled using dynamic factor analysis (DFA; Zuur et al. 2003b), a multivariate technique that can be thought of as an analog to principal component analysis in the time domain. In DFA, response time series are fit with a linear combination of shared, random-walk trends (usually many fewer than the total number of response series), predictors (which can have unique effects on each response series), and random error. We chose DFA over a traditional multivariate state space approach for two reasons. First, it provides advantages in computational efficiency, as a small number of shared trends often adequately capture variation across dozens of responses, and at much lower parameter cost (Zuur et al., 2003a). Second, in terms of identifying what drives the shared trends, having fewer of them allows for greater inferential parsimony. Being a multivariate technique, DFA also provides an advantage over univariate alternatives in that covariance structure among responses can be specified and compared. All models were fit using maximum likelihood estimation by automatic differentiation, with Template Model Builder software (Kristensen et al., 2015), which we called using package TMB in R (R Core Team, 2017; Kristensen et al., 2016).

DFA takes the following form:

$$\mathbf{x}_t = \mathbf{x}_{t-1} + \mathbf{w}_t, \text{ where } \mathbf{w}_t \sim \text{MVN}(0, \mathbf{Q}) \quad (1)$$

$$\mathbf{y}_t = \mathbf{Z}\mathbf{x}_t + \mathbf{D}\mathbf{d}_t + \mathbf{v}_t, \text{ where } \mathbf{v}_t \sim \text{MVN}(0, \mathbf{R}) \quad (2)$$

$$\mathbf{x}_0 \sim \text{MVN}(0, \mathbf{\Lambda}) \quad (3)$$

At time step t , the $m \times 1$ vector of shared trends (\mathbf{x}) is a function of \mathbf{x} in the previous step, plus normal error (\mathbf{w} ; $m \times 1$; Eq. 1). This is the definition of a random walk. The $n \times 1$ response vector (\mathbf{y}) at time t is a function of the shared trends and their factor loadings (\mathbf{Z} ; $n \times m$), covariates (\mathbf{d} ; $q \times 1$) and their river-specific effects (\mathbf{D} ; $n \times q$), and a second normal error term (\mathbf{v} ; $n \times 1$; Eq. 2). \mathbf{R} and \mathbf{Q} are variance-covariance matrices of order m , and \mathbf{Q} is

set to identity for model identifiability (Harvey, 1990). The initial state of the shared trend vector (\mathbf{x}_0) is multivariate-normally distributed with a mean of zero and a diagonal variance-covariance matrix with large variance (e.g. 5; Eq. 3). Response and predictor data were standardized to facilitate comparison of effect sizes and avoid error inflation.

Because we were interested in isolating the effects of climatic predictors on river temperature and discharge, we used fixed factors to absorb recurring seasonal variation not related to the predictors, with one factor level for each month. These factors were incorporated into the covariate matrix (\mathbf{d}). Thus, the coefficient in \mathbf{D} relating, say, air temperature (predictor) and water temperature (response), represents the effect size of the former on the latter. In other words, it is the change in water temperature accompanying a unit change in air temperature across the whole time series. We call this relationship "coupling." We were also interested in coupling by month for specific predictors, which required that the focal predictor in a particular model be arranged seasonally. Concretely,

$$\mathbf{d} = \begin{matrix} & \text{Jan}_{1978} & \text{Feb}_{1978} & \text{Mar}_{1978} & \cdots & \text{Dec}_{2015} \\ \begin{matrix} 1 \\ 2 \\ 3 \\ \vdots \\ 12 \\ 13 \\ 14 \\ 15 \\ 16 \\ \vdots \\ 25 \end{matrix} & \left(\begin{matrix} 1 & 0 & 0 & \cdots & 0 \\ 0 & 1 & 0 & \cdots & 0 \\ 0 & 0 & 1 & \cdots & 0 \\ \vdots & \vdots & \vdots & \ddots & \vdots \\ 0 & 0 & 0 & \cdots & 1 \\ \theta_{precip}^{(1)} & \theta_{precip}^{(2)} & \theta_{precip}^{(3)} & \cdots & \theta_{precip}^{(T)} \\ \theta_{air}^{(1)} & 0 & 0 & \cdots & 0 \\ 0 & \theta_{air}^{(2)} & 0 & \cdots & 0 \\ 0 & 0 & \theta_{air}^{(3)} & \cdots & 0 \\ \vdots & \vdots & \vdots & \ddots & \vdots \\ 0 & 0 & 0 & \cdots & \theta_{air}^{(T)} \end{matrix} \right) \end{matrix}$$

is the covariate matrix structure necessary to account for exogenous seasonal variation (rows 1-12), and overall effect of precipitation (row 13), while also yielding the by-month effect of air temperature (rows 13-24) on the response (\mathbf{y}).

Additional, non seasonal variation due to exogenous effects loads onto the shared trends, and a portion of remaining variation is absorbed by error matrix \mathbf{v} . We fit models using four unique error structures (\mathbf{R}), to allow for different suites of unknown drivers affecting rivers. We included shared variance and zero covariance, individual variance and zero covariance, shared variance and shared covariance, and unconstrained error. Details on these structures and their implications can be found in (Holmes et al., 2012). The best models for water temperature and discharge were determined with AIC.

Landscape predictors and post-hoc regression

For post-hoc analyses, monitoring sites were separated into three classes based on relative areal coverage of perennial ice and/snow (hereinafter “% glaciation”) and mean elevation across their watersheds. The three classes are loosely based on the classification scheme and language of the Climate Impacts Group at the University of Washington (Mauger et al., 2015), and are here delineated according to Table 1.

Table 1 Watershed classification scheme

Classification	Abb.	Glaciation (%)	Mean elev. (m)
Rain-dominated	RD	< 0.7	< 600
Rain-and-snow	RS	< 0.7	≥ 600
Snow-dominated	SD	≥ 0.7	-

After model selection, climatic predictor effect sizes for each river were back-transformed to their original scales and regressed against landscape predictors in order to identify possible watershed-scale controls on coupling. To achieve this, we amassed an additional dataset of landscape features. These were collected individually for each of the watersheds corresponding to our 24 river sites, using the EPA’s StreamCat (stream-catchment) data library (Hill et al., 2016) and the National Hydrography Dataset (NHDPlusV2; McKay et al. 2012). Each site was mapped to an individual river reach, defined as a segment bounded on each end by a stream or river source, confluence, or mouth. The region contributing flow to this reach (its watershed) was then fetched, along with selected areal data, from the NHDPlusV2 database. Landscape attributes used as predictors were aggregated by watershed mean where applicable, and include elevation (m), total area (km²), base flow index, soil permeability (cm hr⁻¹), water table depth (cm), bedrock depth (cm), Base Flow Index (BFI; %), runoff (mm mo⁻¹), percent perennial ice and snow coverage (National Land Cover Database [NLDC] 2006 and 2011 average), riparian population density (people km⁻² within 100m of streams; 2010 census), riparian road density (km km⁻²; 2010 census), and percent riparian urban land (NLCD 2011). Monitoring site elevation (m) and presence of upstream dams (as full/partial/no damming of upstream mainstem and major tributaries) were also included. Finally, we calculated % area over 1000 m (km²), mean slope (percent rise), and mean aspect (degree) by delineating watersheds from a digital elevation model in ArcMap version 10.4 (ArcMap, 2016).

Results

Mean monthly temperature trends for the three river classes, aggregated across all 38 years of data, deviated by a minimum of 1.0°C in December, and a maximum of 3.9°C in July (Fig. 2). SD rivers remained approximately two degrees colder than their RS counterparts through mid-late summer, and 3-4 degrees colder than RD throughout spring and summer. RD rivers were

consistently warmest throughout the year. In January, RS reached a minimum of 4.4°C, and did not significantly differ from SD (Student's t : $p < 0.01$, $F = 11.9$). RD only attained a minimum of 5.6°C. RS reached a peak summer temperature of 16.9°C in July, while RS and SD followed in August with peak temperatures of 15.5 and 13.5°C, respectively.

Meanwhile, the amplitude of T_{air} oscillation exceeded that of any river class, dipping below T_{water} in autumn to a minimum of 3.2°C in December, and rising above RS and SD in March to an August maximum of 17.4°C. T_{air} did not overtake RD T_{water} until August, by which time the latter had begun to decline.

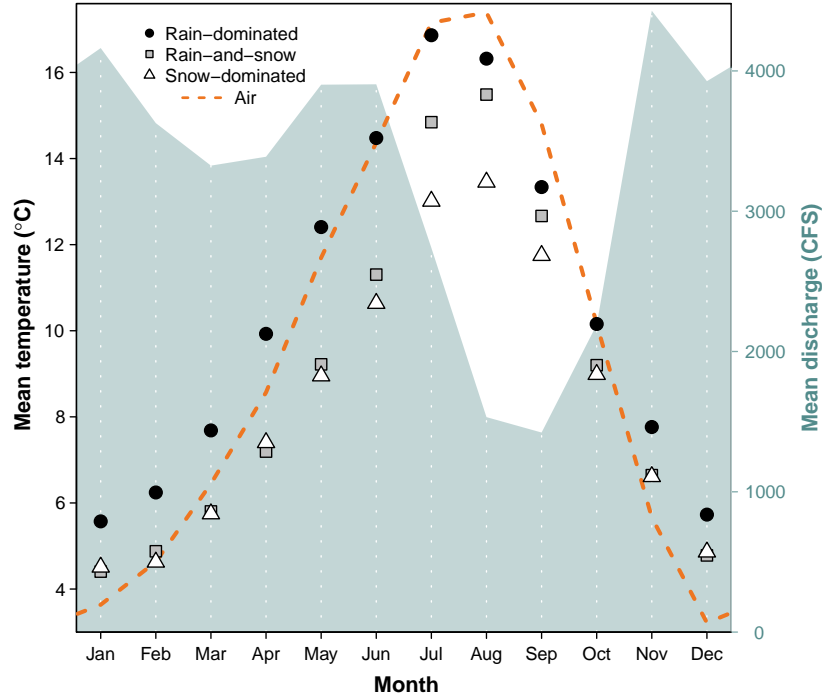


Figure 2 Monthly mean T_{water} by river class, and T_{air} and Q across classes, from 1978 to 2015. All depicted series represent discrete data.

The combined hydrograph of all rivers revealed two primary peaks, one beginning in late spring and the other extending from late fall to early winter, with a prominent trough in late summer. Spring peak discharge coincided noticeably with a separation in water temperature between SD and RS, while the

summer trough coincided with separation of RD and T_{air} . On average, November marked both the autumn peak in discharge and the point at which T_{air} fell below T_{water} .

There was also an apparent divergence in slope between RD and all snow-influenced rivers, beginning in early spring and culminating in June. Between June and July, RS and SD saw a large jump in temperature, which coincided with the decline in snowmelt.

DFA results, aggregated across months and years for each site, revealed a trend toward reduced $T_{\text{air}} \rightarrow T_{\text{water}}$ coupling with increasing watershed elevation ($p = 0.04, R^2 = 0.18$; Fig. 3a). On average, a 1°C change in T_{air} corresponded to a $0.53 \pm 0.03^\circ\text{C}$ change in T_{water} at RD, a $0.51 \pm 0.08^\circ\text{C}$ change at RS, and a $0.45 \pm 0.17^\circ\text{C}$ change at SD sites. A similar trend was observed with respect to $\text{Precip} \rightarrow T_{\text{water}}$ coupling ($p = 0.03, R^2 = 0.21$; Fig. 3b), where a monthly change in total precipitation of 1 cm corresponded to a $0.02 \pm 0.009^\circ\text{C}$ change in T_{water} for RD, $-0.003 \pm 0.009^\circ\text{C}$ for RS, and $0.004 \pm 0.02^\circ\text{C}$ for SD. There was no evidence of coupling between snowmelt and T_{water} (Fig. 3c), but this predictor was included in the most parsimonious DFA model selected via AIC and R^2 (See Appendix A.). It is of note that the strongest examples of $T_{\text{air}} \rightarrow T_{\text{water}}$ and $\text{Precip} \rightarrow T_{\text{water}}$ coupling were observed in the Duckabush River, while the weakest examples are from the Elwha River. Both rivers drain glaciers of the Olympic Mountain Range, and both are SD, though the Elwha's watershed is larger.

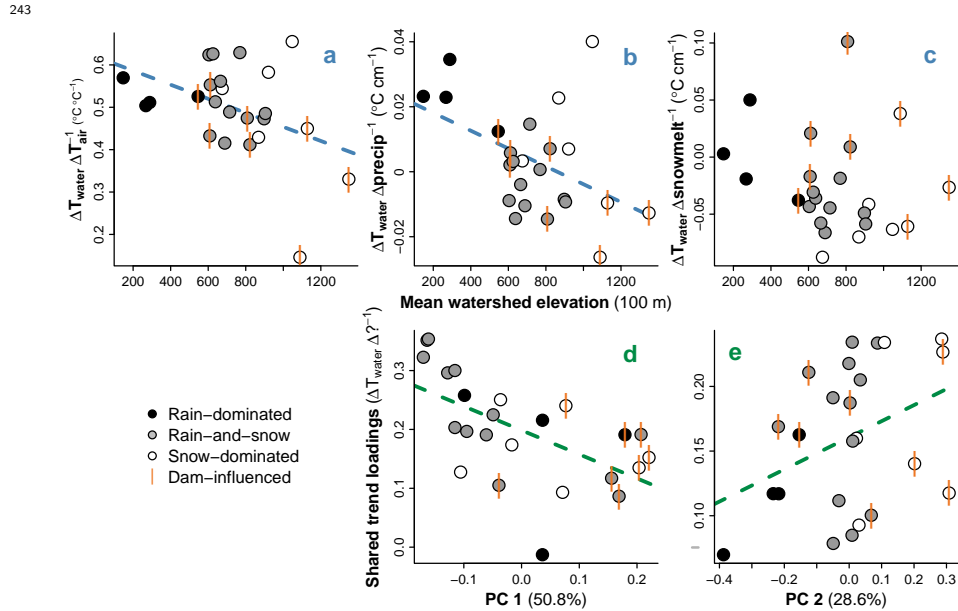
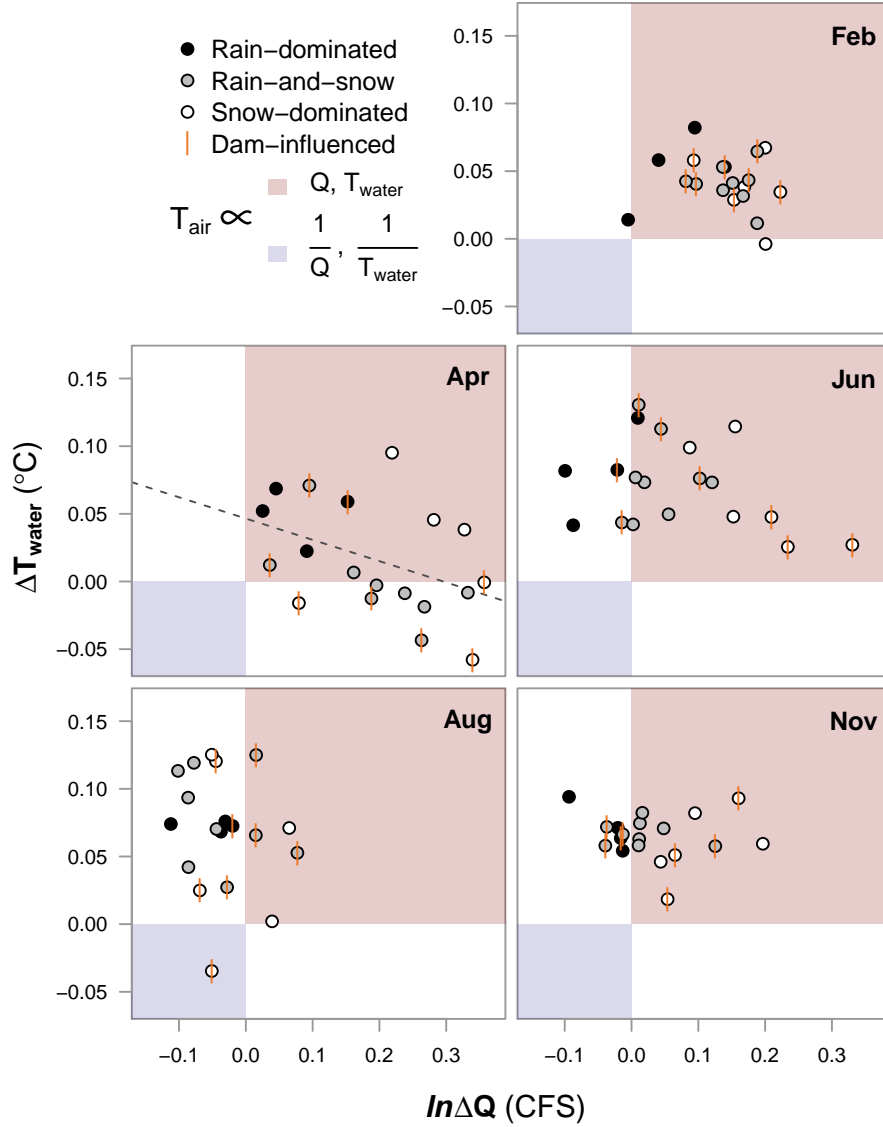


Figure 4 Relationships between watershed elevation and climatic effects on

246 T_{water} (**a-c**), and between watershed features and factor loadings on shared
247 trends (**d-e**). Regression lines indicate slopes significant at $\alpha = 0.1$.

248 In addition to the three climate predictors above, the best T_{water} model
249 also included five shared trends. Of these, four correlated significantly with at
250 least one known watershed predictor. Figure 3 depicts the strongest correlated
251 variables with each trend (insets d-e). These are, in arbitrary order of relevance,
252 mean water table depth ($p < 0.001$, $R^2 = 0.60$; Fig. 3d), % glaciation ($p <$
253 0.01 , $R^2 = 0.30$; Fig. 3e), BFI ($p = 0.01$, $R^2 = 0.25$; Fig. 3f), and mean slope
254 ($p < 0.01$, $R^2 = 0.29$; Fig. 3g). The fifth shared trend was not correlated with
255 any variables in the watershed predictor dataset.

256



257

258 **Figure 4** Relationship between $T_{air} \rightarrow T_{water}$ and $T_{air} \rightarrow Q$. Both axes are
 259 expressed per $1^{\circ}C$ change in T_{air} . The red quadrant designates proportionality
 260 between all three variables, the blue inverse proportionality between each
 261 response and T_{air} . Regression lines indicate slopes significant at $\alpha = 0.05$.

262 To examine possible sub-season interactions between T_{air} , T_{water} and Q , we
 263 performed an additional DFA with Q as the response. In both models, T_{air} was
 264 allowed to have unique monthly effects. These effects, taken together, can be
 265 understood in relation to the four quadrants of the Cartesian coordinate system

(increasing clockwise from upper right; Fig. 4).

In mid-winter (exemplified by February), all river classes primarily occupy the first quadrant, signifying $T_{\text{air}} \propto T_{\text{water}}$ and $T_{\text{air}} \propto Q$, where \propto denotes proportionality. RD shows the weakest Q response. By spring, many RS and SD sites develop an inverse relationship between T_{air} and T_{water} , denoted $T_{\text{air}} \propto \frac{1}{T_{\text{water}}}$, while RD sites change little from their winter state. June and August see a procession of most sites into the near fourth quadrant, with SD trailing. This signifies $T_{\text{air}} \propto \frac{1}{Q}$, though $T_{\text{air}} \propto T_{\text{water}}$ remains. One stark exception is again the Elwha river, which occupies quadrant three. By fall, RS and SD have begun progress back toward their winter states, led by SD. RD, meanwhile, remain essentially unmoved from summer.

Discussion

The effects of climate on T_{water} , determined by dynamic factor analysis, suggest that nearly all rivers included in our dataset were influenced strongly by air temperature, precipitation, and/or snowmelt across 38 years of monthly data (Fig. 3). At most monitoring sites, T_{water} closely tracked changes in T_{air} , on average responding to increases and decreases with proportional movements of up to 66% magnitude. However, some rivers only weakly track T_{air} , and several patterns in the intensity of this coupling correlate strongly with watershed features relating to ice, groundwater, and slope. Glaciation and yearly snow burden are prominent among these, and for reasons of ecological and hydrological implication, the primary focus of the following discussion.

Without any analysis, a "buffering" effect (hereinafter contrasted with "coupling") of ice on river temperature can be seen in the yearly patterns of T_{water} relative to T_{air} (Fig. 2). The aggregate hydrograph peaks due to snowmelt from April to June, at the same time that the trajectories of RS and SD (snow-influenced rivers) start to drop off relative to RD. After snowmelt begins to subside, RS and SD recover with a noticeable jump. For rivers that receive glacial runoff (SD), this effect appears to remain, buffering them from summer temperature rise where RS rivers instead take on the character of RD (Fig. 4). In an extreme case, the Elwha River was actually cooler in August during those years in which air temperature was higher, likely due to increased runoff from Carrie and Eel glaciers. The buffering effect of ice on river temperature is therefore two-fold, acting first on all snowmelt-influenced rivers through a cold-water pulse in spring, and then on a subset of those rivers throughout summer and fall, by way of glacial runoff. For RD rivers, which receive little to no input from ice, summer temperature is entirely dictated by that of the surrounding air, and whatever rain falls through it. Though higher-elevation watersheds will always produce colder water, independent of the influence of ice, it can be expected that RS and SD rivers will grow more similar to RD as regional temperatures warm and glaciers decline. That is to say, formerly reliably cold-water

streams and associated habitats may see increases in both summer and winter average temperatures, as well as higher variability from year to year. The Elwha in particular may slip from its current state of high resistance to seasonal climatic changes. We tested for changes in mean and variance of $T_{\text{air}} \rightarrow T_{\text{water}}$ and $T_{\text{air}} \rightarrow Q$ coupling between 1978 and 2015, but did not detect any regular patterns (Appendix B).

In addition to the three climate predictors, five shared trends were fit by the most parsimonious DFA model. These represent additional drivers responsible for structuring water temperature across some or all of the 24 sites included in the analysis. Each monitoring sites' factor loading on a particular shared trend indicates the degree to which the trend accounted for variance in T_{water} at that site. While the precise identities of these drivers cannot be obtained with certainty, they can be inferred through correlation with predictor variables. In this way, we determined the most likely landscape drivers of T_{water} to be perennial ice and snow cover, mean watershed slope, and groundwater influx. In the case of slope, the likely mechanism of influence is increased turbulence and mixing of water and air in steep, headwater streams, which allows convective warming and cooling to occur more rapidly Brutsaert 1975; Fig. 3g). As for groundwater, greater influx (represented by baseflow index, or BFI; fig. 3f) corresponds to greater *de*-coupling of climatic effects and river temperature, as groundwater should be insulated relative to surface water. For the same reason, greater depth of groundwater should be associated with better insulation and thus further decoupling (Fig. 3d). The buffering effect of perennial ice and snow on SD rivers has already been discussed, but the uniquely high factor loadings of RS rivers in relation to the associated trend are worth noting (Fig. 3e). This trend may account for variation in RS due to traits shared by RD and SD, or to a "rain-on-snow" effect that may yield additional cold water in early spring. The fifth trend did not correlate strongly with any of the landscape predictors in our dataset. It may therefore represent additional, unknown drivers like marine or microclimatic effects, or it may simply account for random noise.

The relationship between climate and river temperature is further influenced by the interaction of discharge, and the fates of rivers in the Puget Sound watershed can be best understood by examining these factors in combination (Fig. 4). Whether rain-, both-, or snow-dominated, all rivers took on RD characteristics in winter, when the effects of ice lay latent. As a result, warmer Februaries on average yielded warmer rivers and higher flow (less precipitation bound in ice). The critical differences between river classes played out in spring and summer, and it's during these months that future perturbations due to changing climate may be felt most acutely. For example, warmer Aprils on average produced colder water at 9 out of 15 RS and SD sites. Though we determined discharge, groundwater, and slope to be likely components of this relationship, only melting ice could be credited with actually reversing it. Projected reductions in snow-pack for the Pacific Northwest can therefore be expected to fundamentally alter the responses of currently snow-influenced rivers to yearly variation in spring temperature. In the longer term, changes can be expected for rivers that now

352 receive the temperature-buffering effect of glacial runoff. Glaciers continue to
353 decline across North America, with glacial ice across Western Canada projected
354 to decline by 70% from 2005 to 2100 (Clarke et al., 2015).

355 Conclusion

356 Temperature regimes across the rivers of the Puget Sound watershed are struc-
357 tured by a combination of climatic drivers at the regional scale, and geophysical
358 drivers at watershed scales. In the absence of snow and ice, river temperature is
359 closely coupled to that of the surrounding air, while contributions of snowmelt
360 and glacial runoff can dampen or even reverse this coupling in spring and sum-
361 mer. In some cases, icemelt-influenced rivers exhibit stronger positive responses
362 to climate patterns than their rain-driven counterparts. Our results suggest el-
363 evational variations in groundwater influx, total discharge, and watershed slope
364 account for these patterns. However, while these factors may influence the de-
365 gree of coupling between climatic drivers and water temperature, only snow
366 and ice can reverse it. Since 1978, such reversals have been widespread, par-
367 ticularly during spring melt. Though we did not detect changes in this effect
368 across historical observations, future reductions in snowpack and glacial mass
369 are projected. Consequently, many rivers that now undergo the mildest seasonal
370 temperature changes may be impacted most strongly.

References

- ArcMap (2016). Environmental systems research institute (esri). *Redlands, CA*: <http://www.esri.com/>.
- Boisneau, C., Moatar, F., Bodin, M., and Boisneau, P. (2008). *Does global warming impact on migration patterns and recruitment of Allis shad (Alosa alosa L.) young of the year in the Loire River, France?*, pages 179–186. Springer Netherlands, Dordrecht.
- Boscarino, B. T., Rudstam, L. G., Mata, S., Gal, G., Johannsson, O. E., and Mills, E. L. (2007). The effects of temperature and predatorprey interactions on the migration behavior and vertical distribution of mysis relicta. *Limnology and Oceanography*, 52(4):1599–1613.
- Brutsaert, W. (1975). A theory for local evaporation (or heat transfer) from rough and smooth surfaces at ground level. *Water resources research*, 11(4):543–550.
- Carter, K. (2005). The effects of temperature on steelhead trout, coho salmon, and chinook salmon biology and function by life stage. *Implications for the Klamath River total maximum daily loads. California Regional Water Quality Control Board. North Coast Region, Santa Rosa, California*.
- Clarke, G. K., Jarosch, A. H., Anslow, F. S., Radić, V., and Menounos, B. (2015). Projected deglaciation of western canada in the twenty-first century. *Nature Geoscience*, 8(5):372–377.
- Eldridge, E. (1967). Water temperature: influences, effects, and control. Technical report, Federal Water Pollution Control Administration, Portland, Oreg.(USA). Northwest Region.
- Garner, G., Hannah, D. M., Sadler, J. P., and Orr, H. G. (2014). River temperature regimes of england and wales: spatial patterns, inter-annual variability and climatic sensitivity. *Hydrological Processes*, 28(22):5583–5598.
- Harvey, A. C. (1990). *Forecasting, structural time series models and the Kalman filter*. Cambridge university press.
- Hill, R. A., Weber, M. H., Leibowitz, S. G., Olsen, A. R., and Thornbrugh, D. J. (2016). The stream-catchment (streamcat) dataset: A database of watershed metrics for the conterminous united states. *JAWRA Journal of the American Water Resources Association*, 52(1):120–128.
- Holmes, E. E., Ward, E. J., and Wills, K. (2012). Marss: Multivariate autoregressive state-space models for analyzing time-series data. *The R Journal*, 4(1):11–19.
- Kristensen, K., Nielsen, A., Berg, C. W., Skaug, H., and Bell, B. (2015). Tmb: automatic differentiation and laplace approximation. *arXiv preprint arXiv:1509.00660*.

410 Kristensen, K., Nielsen, A., Berg, C. W., Skaug, H., and Bell, B. M. (2016).
 411 TMB: Automatic differentiation and Laplace approximation. *Journal of Sta-*
 412 *tistical Software*, 70(5):1–21.

413 Lisi, P. J., Schindler, D. E., Bentley, K. T., and Pess, G. R. (2013). Association
 414 between geomorphic attributes of watersheds, water temperature, and salmon
 415 spawn timing in alaskan streams. *Geomorphology*, 185:78–86.

416 Lisi, P. J., Schindler, D. E., Cline, T. J., Scheuerell, M. D., and Walsh, P. B.
 417 (2015). Watershed geomorphology and snowmelt control stream thermal sen-
 418 sitivity to air temperature. *Geophysical Research Letters*, 42(9):3380–3388.

419 Mauger, G., Casola, J., Morgan, H., Strauch, R., Jones, B., Curry, B., Isak-
 420 sen Busch, T., et al. (2015). State of knowledge: Climate change in puget
 421 sound.

422 McCullough, D. A. (1999). *A review and synthesis of effects of alterations to the*
 423 *water temperature regime on freshwater life stages of salmonids, with special*
 424 *reference to Chinook salmon*. US Environmental Protection Agency, Region
 425 10.

426 McKay, L., Bondelid, T., Dewald, T., Johnston, J., Moore, R., and Rea, A.
 427 (2012). Nhdplus version 2: user guide. *National Operational Hydrologic Re-*
 428 *remote Sensing Center, Washington, DC*.

429 Mote, P. W. and Salathe, E. P. (2010). Future climate in the pacific northwest.
 430 *Climatic Change*, 102(1-2):29–50.

431 NOAA (2017). National centers for environmental information, climate at a
 432 glance: U.s. time series. Data retrieved from: [http://www.ncdc.noaa.gov/](http://www.ncdc.noaa.gov/cag/)
 433 [cag/](http://www.ncdc.noaa.gov/cag/) on 11/10/2016.

434 Poole, G. C. and Berman, C. H. (2001). An ecological perspective on in-
 435 stream temperature: natural heat dynamics and mechanisms of human-
 436 caused thermal degradation. *Environmental management*, 27(6):787–802.

437 R Core Team (2017). *R: A Language and Environment for Statistical Comput-*
 438 *ing*. R Foundation for Statistical Computing, Vienna, Austria.

439 Radeloff, V. C., Nelson, E., Plantinga, A. J., Lewis, D. J., Helmers, D.,
 440 Lawler, J., Withey, J., Beaudry, F., Martinuzzi, S., Butsic, V., et al. (2012).
 441 Economic-based projections of future land use in the conterminous united
 442 states under alternative policy scenarios. *Ecological Applications*, 22(3):1036–
 443 1049.

444 Reidy Liermann, C., Olden, J. D., Beechie, T., Kennard, M. J., Skidmore,
 445 P., Konrad, C., and Imaki, H. (2012). Hydrogeomorphic classification of
 446 washington state rivers to support emerging environmental flow management
 447 strategies. *River Research and Applications*, 28(9):1340–1358.

- 448 USDA (2017). National resources conservation service. Data retrieved
449 from: [https://www.nrcs.usda.gov/wps/portal/nrcs/detail/or/snow/](https://www.nrcs.usda.gov/wps/portal/nrcs/detail/or/snow/?cid=nrcs142p2_046350)
450 [?cid=nrcs142p2_046350](https://www.nrcs.usda.gov/wps/portal/nrcs/detail/or/snow/?cid=nrcs142p2_046350) on 1/23/2017.
- 451 USGS (2017). National water information system. Data retrieved from: [http:](http://www.ecy.wa.gov/programs/eap/fw_riv/index.html)
452 [//www.ecy.wa.gov/programs/eap/fw_riv/index.html](http://www.ecy.wa.gov/programs/eap/fw_riv/index.html) on 1/30/2017.
- 453 van Vliet, M. T., Franssen, W. H., Yearsley, J. R., Ludwig, F., Haddeland, I.,
454 Lettenmaier, D. P., and Kabat, P. (2013). Global river discharge and water
455 temperature under climate change. *Global Environmental Change*, 23(2):450–
456 464.
- 457 Von Prause, M. (2017). River and stream water quality monitoring program.
458 Data retrieved from Washington Department of Ecology: [http://www.ecy.](http://www.ecy.wa.gov/programs/eap/fw_riv/index.html)
459 [wa.gov/programs/eap/fw_riv/index.html](http://www.ecy.wa.gov/programs/eap/fw_riv/index.html) on 7/1/2016.
- 460 Ward, J. (1985). Thermal characteristics of running waters. In *Perspectives in*
461 *Southern Hemisphere Limnology*, pages 31–46. Springer.
- 462 Zuur, A., Tuck, I., and Bailey, N. (2003a). Dynamic factor analysis to estimate
463 common trends in fisheries time series. *Canadian journal of fisheries and*
464 *aquatic sciences*, 60(5):542–552.
- 465 Zuur, A. F., Fryer, R., Jolliffe, I., Dekker, R., and Beukema, J. (2003b). Estimat-
466 ing common trends in multivariate time series using dynamic factor analysis.
467 *Environmetrics*, 14(7):665–685.

468 **Appendix A**

469 **Temperature DFA output and diagnostics**

470 Model selection included four climate covariates (air temperature, precipita-
471 tion, snowmelt, and hydrological drought), between 1 and 15 shared trends,
472 four within-and-among-site error structures (see methods), and two models of
473 unknown seasonal variation (fixed monthly factors and Fourier series). The
474 most parsimonious model of river temperature was selected using the Akaike
475 Information Criterion (AIC), and included air temperature, precipitation, and
476 snowmelt as covariates. This model also included five shared trends and an inde-
477 pendent and unequally distributed error structure among streams (i.e. diagonal
478 and unequal variance-covariance matrix).

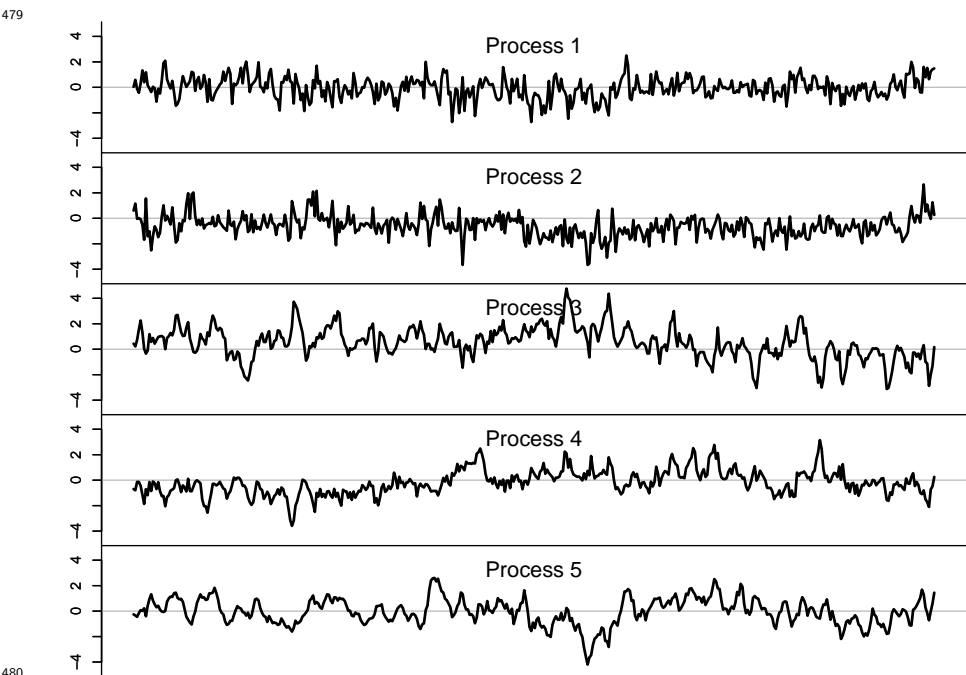


Figure A1 Shared trends.

482

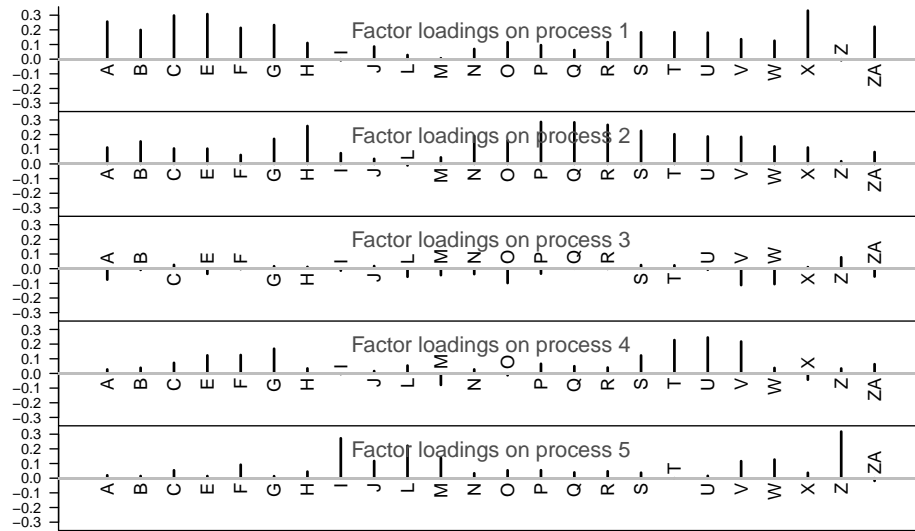


Figure A2 Factor loadings on shared trends.

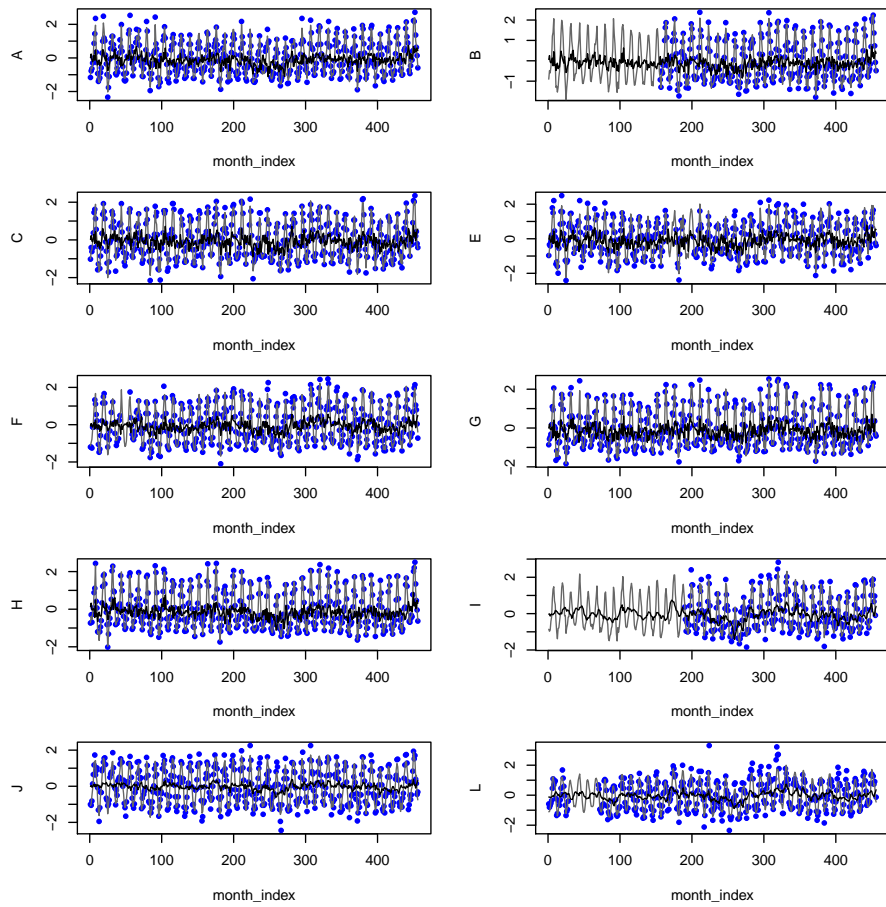


Figure A3 Model fits (gray line = overall; black line = trends-only).

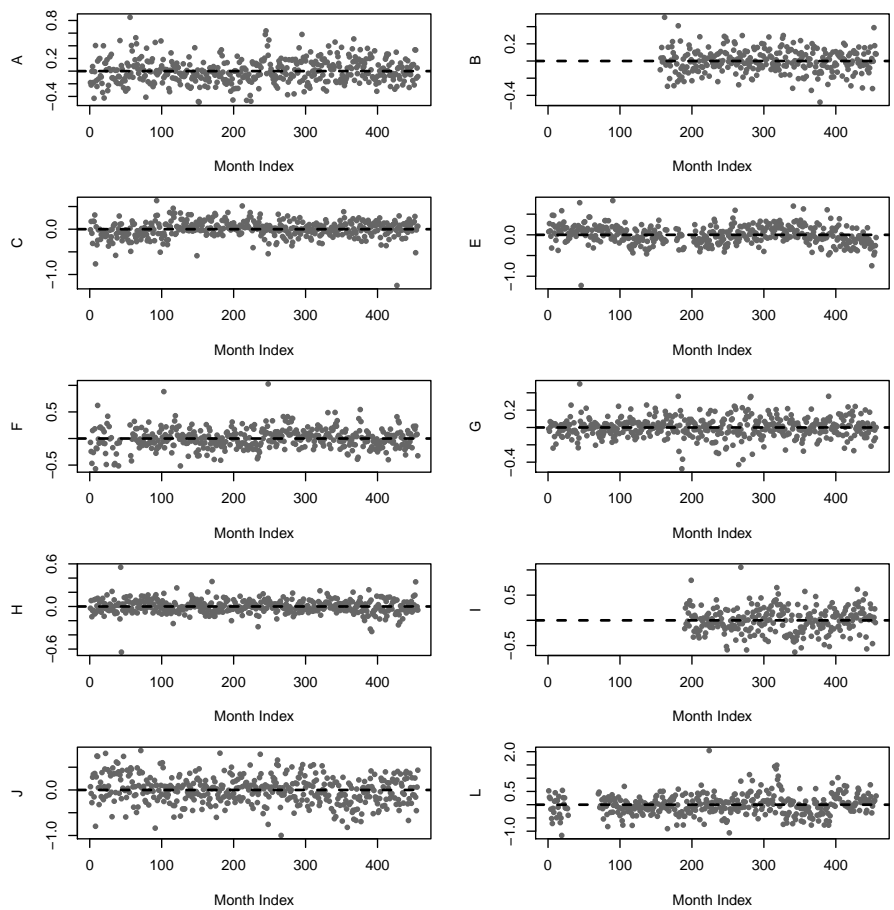


Figure A4 Residuals.

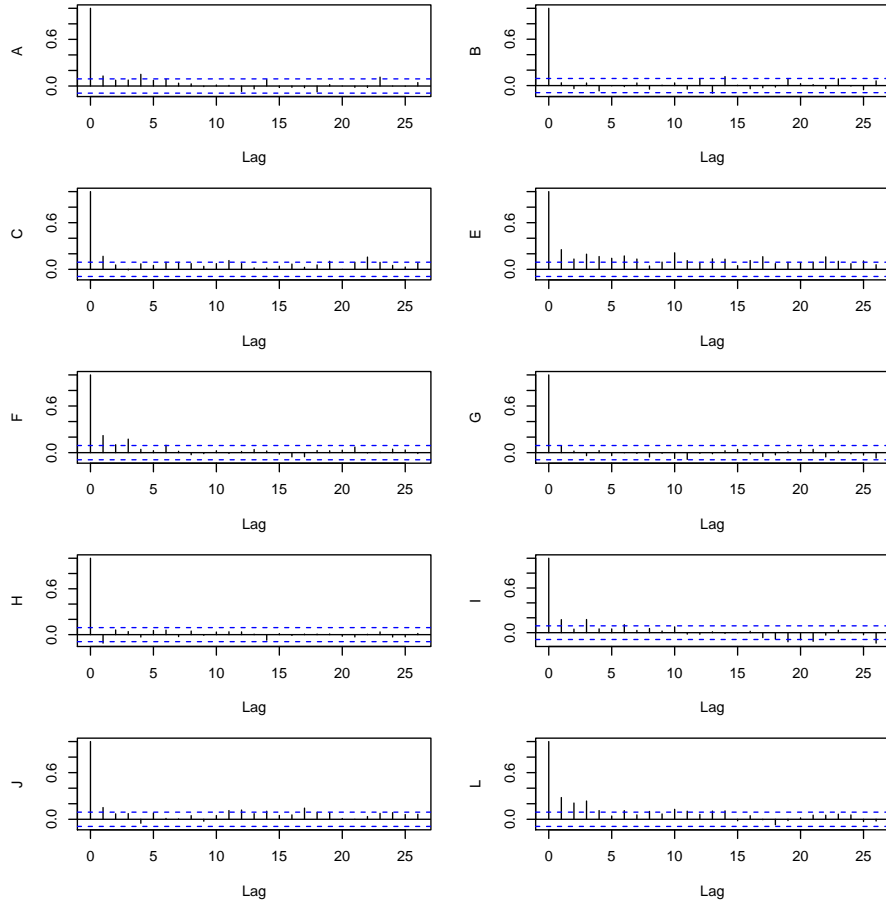


Figure A5 Autocovariance function (ACF).

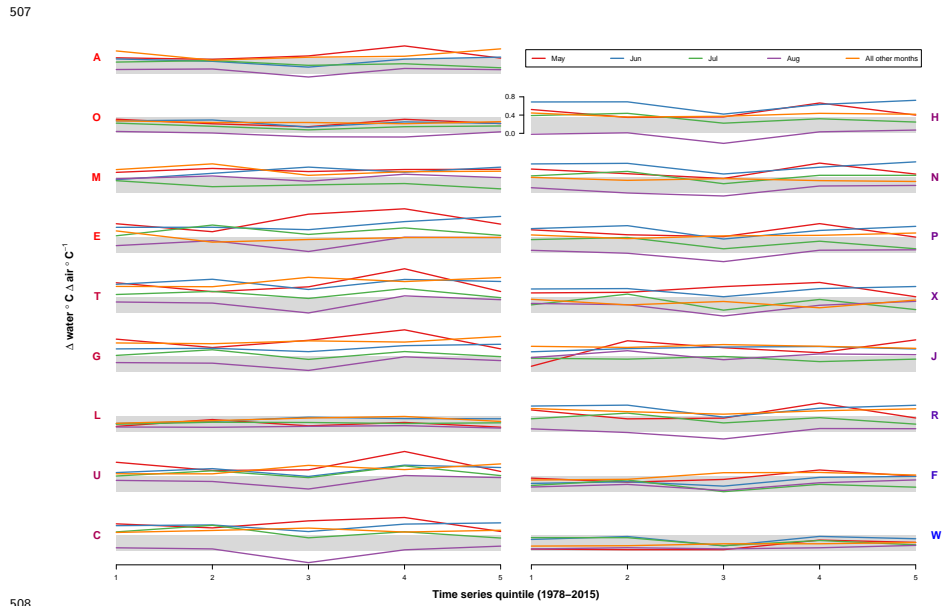
Output from the discharge model looks very similar to this, and is omitted here for the sake of retaining a reasonable page count.

496 Appendix B

497 Testing for change in coupling over time

498 We used an additional DFA model to test for changes in $T_{air} \rightarrow T_{water}$ coupling
 499 over time, by dividing the 1978-2015 time series into 5 intervals and comparing
 500 central tendency and variance of effect sizes for each interval. Figures B1-B3
 501 show mean effect size for each stream.

502 To approximate estimates of variability over time, we performed the same
 503 analysis within a Bayesian framework, and obtained uncertainty estimates from
 504 the credible intervals of the effect size posteriors. This approach yielded no
 505 trends in variation over time, and is not visualized here (This will be included
 506 in the final version of this paper).



508 **Figure B1** Mean $T_{air} \rightarrow T_{water}$ coupling over time. Each plot corresponds to
 509 an individual site. Y-label colors represent mean watershed elevation
 510 (bluer=higher).
 511

512

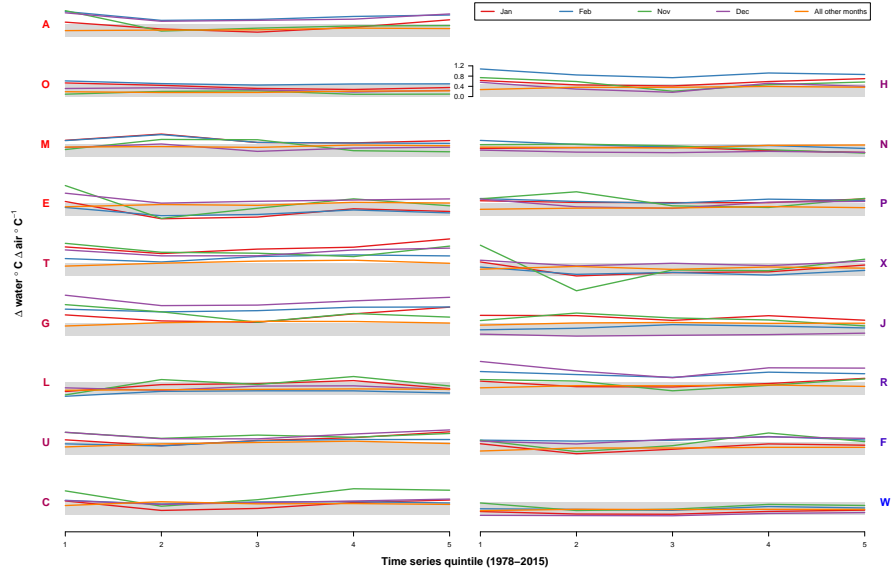


Figure B2 Mean $T_{air} \rightarrow T_{water}$ coupling over time. Each plot corresponds to an individual site. Y-label colors represent mean watershed elevation (bluer=higher).

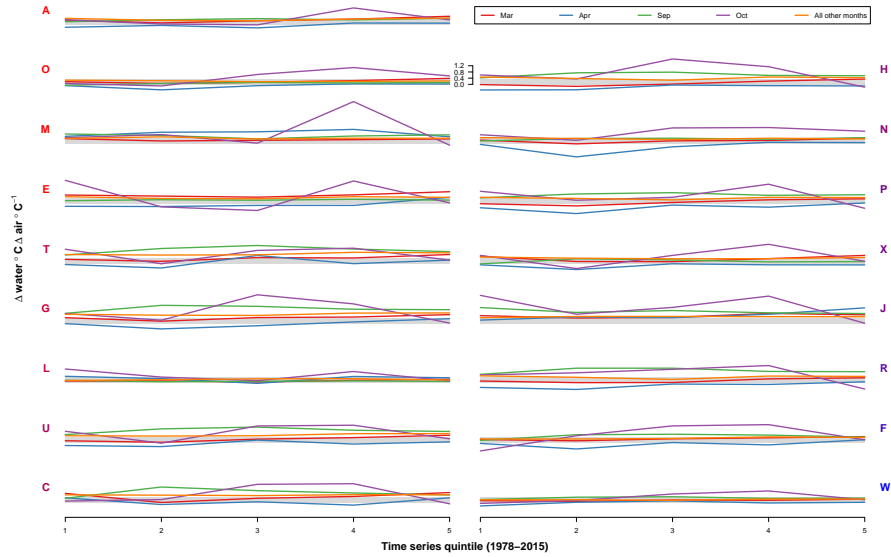


Figure B3 Mean $T_{air} \rightarrow T_{water}$ coupling over time. Each plot corresponds to an individual site. Y-label colors represent mean watershed elevation (bluer=higher).